

Received 4 June 2025, accepted 17 June 2025, date of publication 19 June 2025, date of current version 27 June 2025.

Digital Object Identifier 10.1109/ACCESS.2025.3581502

RESEARCH ARTICLE

Coupled Induction Machine and HVAC Models for Simulating HVAC Performance Considering Grid Dynamics in Buildings

VISWANATHAN GANESH¹, ZHANWEI HE¹, JIANJUN HU²,
SEN HUANG³, AND WANGDA ZUO^{1,4}

¹Department of Architectural Engineering, The Pennsylvania State University, University Park, PA 16802, USA

²Lawrence Berkeley National Laboratory, Berkeley, CA 94720, USA

³Oak Ridge National Laboratory, Oak Ridge, TN 37830, USA

⁴National Renewable Energy National Laboratory, Golden, CO 80401, USA

Corresponding author: Wangda Zuo (wangda.zuo@psu.edu)

This work was supported in part by the DOE's Office of Energy Efficiency and Renewable Energy through the Advanced Manufacturing Office, under Award DE-EE0009139; and in part by the National Renewable Energy Laboratory, operated by Alliance for Sustainable Energy, LLC, for U.S. Department of Energy (DOE) under Contract DE-AC36-08GO28308.

ABSTRACT This paper presents the development of novel models that integrate induction machines with HVAC equipment, such as pumps, heat pumps, and chillers, to analyze the impact of electrical parameters on the operational performance of thermo-fluid systems. The proposed model employs a coupling technique that captures the dynamic interactions between induction machines and HVAC systems. By integrating electrical, thermal, and mechanical dynamics, the models provide a comprehensive framework for simulating real-world scenarios, including interactions with the electrical grid. This achievement was made possible through the development of a Computationally Efficient and Accurate Induction Machine (CEAIM) model. Implemented using the equation-based Modelica language, the CEAIM model has been validated against experimental results, manufacturer data sheets, and various operating conditions. Its performance has been compared with existing induction machine models in the Modelica Standard Library (MSL), demonstrating superior accuracy and computational efficiency. The CEAIM model predicts torque, speed, and power consumption with a coefficient of determination (R^2) ranging from 0.98 to 1 and a coefficient of variation of root mean square error (CVRMSE) between 0.27% and 6.67%. Additionally, CEAIM scales more efficiently than conventional MSL models, with a slower computational growth rate in large-scale simulations. After thorough validation of the CEAIM model, it was coupled with HVAC equipment as this approach provides a detailed multi-dimensional view of capturing electrical transients and mechanical performance. To support this, a case study was conducted to showcase its capabilities.

INDEX TERMS Chiller, grid interactive, heat pump, induction machine, pump.

I. INTRODUCTION

Initially predominant in industrial settings, induction machines are now integral to various applications, including within buildings. For example, induction machines are increasingly employed in heating, ventilation, and air conditioning (HVAC) systems, elevators, and other building services that necessitate efficient power management. Their

The associate editor coordinating the review of this manuscript and approving it for publication was Agustin Leobardo Herrera-May.¹

integration into building management systems is vital for optimizing energy use, minimizing operational costs, and enhancing overall building performance. This integration not only contributes to energy efficiency but also plays a role in the comfort and safety of building occupants.

This reliance on induction machines within the building sector is a crucial step towards their strategic role in the larger context of grid interactive applications. The concept of Building-to-Grid (B2G) integration represents a transformative approach to energy management, enabling

buildings to change from passive energy consumers into dynamic and interactive energy grid components. In this paradigm, buildings actively respond to grid conditions, such as voltage drops, by adapting their energy consumption and operational performance. Induction machines are pivotal in this context, ensuring efficient energy transfer and maintaining operational stability under varying grid conditions. Their ability to sustain performance during voltage fluctuations is critical for grid resilience, allowing buildings to support grid stability and contribute to a more flexible and robust energy infrastructure.

The complexity and dynamic nature of B2G systems necessitate an accurate and efficient modeling of induction machines. Modeling is crucial as it enables the prediction and optimization of machine performance in dynamic scenarios, ensuring systems can efficiently respond to varying demands from both buildings and the grid. A comprehensive model also enhances the understanding of complex interactions between machines, building systems, and the grid, facilitating the development of energy-efficient and sustainable strategies. Additionally, modeling allows for scenario simulation, supporting informed decision-making in building design and grid integration. Developing a model that accurately represents the complex dynamics of induction machines in B2G systems presents several challenges. B2G applications care about variables like terminal voltage, current, power factor, and power consumption. The building and energy industry practice requires fast computing speed, like completing an annual simulation within a few minutes.

Several existing models provide steady or quasi-transient state analysis which considers the operation condition and responses to resemble steady state to avoid using complex calculations [1]. However, this steady state assumption can only be suitable for mechanical devices such as chillers, cooling towers, etc., as they have a response time of minutes to hours. The slow response time is not valid for electrical equipment such as electric motors. In such applications, the steady-state models fail to consider the dynamic nature of voltage, current, power factor, and dynamic responses to slight changes in the set point since these factors tend to change in periods of milliseconds to seconds.

As identified in the above literature review, there is a gap in models that can achieve both high accuracy and computational efficiency for induction machines in B2G applications. We propose a new Computationally Efficient and Accurate Induction Machine (CEAIM) model by combining circuit theory with parametric methods that can be coupled with mechanical devices like pumps, chillers and heat pump to simulate multi-domain models. This approach bypasses the direct simulation of power electronic transitions by substituting them with sophisticated mathematical approximations as they consider the interaction of current and voltage through the basic circuit elements such as resistor, inductor and capacitor using circuit theory and having predefined circuit parameters from the product database thereby optimizing computational efficiency.

The rest of paper is outlined as follows: Section II provides an introduction to the induction machine, Section III develops an induction machine model using mathematical equations, Section IV details the implementation of this model in Modelica, Section V presents the validation results, Section VI discusses a comparison of the simulation results between the proposed model and a counterpart from Modelica Standard Library, Section VII presents a case study of grid dynamics when proposed induction machine is coupled with pump, heat pump and chillers and Section VIII concludes the study.

II. OVERVIEW OF INDUCTION MACHINE

To explain the new CEAIM model, this section provides an overview of the physical components, control techniques, and existing approaches to model induction machines.

A. PHYSICAL COMPONENT

Induction machines are electromechanical systems consisting of several key components including stator, rotor, bearings, shaft, and cooling system (Figure 1). The stator is the stationary outer part consisting of a cylindrical frame and a laminated iron core with slots for stator windings. These windings are usually three-phase coils connected in a star or delta configuration and responsible for producing a rotating magnetic field when AC power is supplied [2]. Located inside the stator, rotor is the rotating part of the machine. The most common rotor is squirrel-cage rotor, consisting of aluminum or copper bars short-circuited by end rings. As the stator's magnetic field rotates, it induces a current in the rotor, creating a secondary magnetic field that interacts with the stator field to produce torque [2]. Other parts include bearings [3] and cooling systems [4].

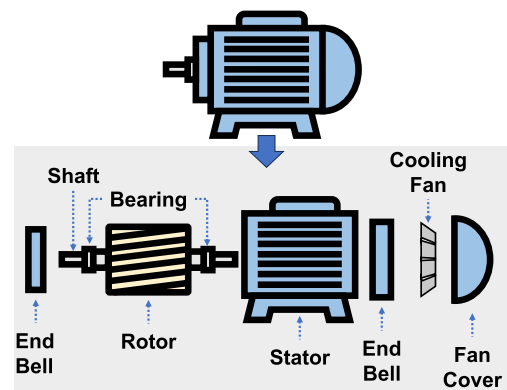


FIGURE 1. Induction machine physical components.

B. CONTROL TECHNIQUES

The control of induction machines is vital for their efficient operation, especially in applications requiring precise speed and torque control. The primary method for controlling the speed of an induction motor involves voltage/frequency control. By adjusting the voltage and frequency supplied to the motor, its speed can be varied. This method is simple

and cost-effective but offers limited control over torque and speed [5], [6]. Other prominent techniques used are vector control [7], [8] and direct torque control [9].

C. INDUCTION MACHINE MODELING

Modeling induction machine is essential for understanding their behavior and designing efficient control systems. Induction machine modeling involves creating mathematical representations to simulate their performance under various operating conditions. The complexity of these models varies, ranging from simple equivalent circuit models to complex finite element models that account for various physical phenomena [1] depending on their applications.

The induction machine modeling can be broadly classified into physics-based, data-driven and analytical models, where physics-based model are generally circuit-based models use equivalent electrical circuits to represent the induction machine. These models typically include representations of the stator and rotor resistances and inductances, and sometimes mutual inductance, to simulate the machine's electromagnetic behavior. They are widely used due to their relative simplicity and effectiveness in capturing the essential dynamics of induction machines. Data-driven models rely on machine data to predict behavior and do not necessarily adhere to the physical principles of the machine. For example, Finite element models (FEM) use numerical techniques to solve the physical equations governing the operation of induction machines. These models provide detailed insights into the electromagnetic, thermal, and mechanical behavior of the machine, making them suitable for design and analysis of complex applications.

Analytical models are based on the fundamental principles governing the operation of induction machines. These mathematical models are used for theoretical analysis, design, and performance prediction. They often involve solving differential equations that describe the machine's electromagnetic and mechanical dynamics. In recent years, machine learning models, particularly neural networks, use computational algorithms based on the analytical model to predict the behavior of the machine based on historical data. These models are becoming increasingly popular due to their ability to handle complex, nonlinear relationships and adapt to changing conditions. Therefore, the first step of modeling an induction machine is to define the usage of the model and related physical characteristics. Then we can construct/select the models accordingly. Typically, models for induction machine can be categorized into analytical models, data-driven models, physics-based model and parameter estimation models as shown in Table 1.

TABLE 1. Categories of induction machine models.

Model Category	References
Analytical models	[10]–[23]
Data-driven models	[12]–[14], [24]–[33]
Physics-based models	[19], [31], [34]–[39]
Parameter estimation models	[11], [15], [27], [36]–[46]

D. GAPS AND LIMITATIONS

The complex requirements of modeling for a B2G system emphasize the need to capture both transient and steady-state characteristics within a single model. Transient responses refer to the system's reaction to sudden changes, such as power outages or demand spikes. These require detailed, time-sensitive simulations to accurately predict voltage and current fluctuations. Such simulations are computationally intensive because they must resolve the electrical behavior at very small time intervals, often in the order of microseconds to milliseconds. For example, during a power outage, the system's ability to maintain stable operation depends on how quickly it can respond to the sudden loss of power. These quick responses can reveal vulnerabilities or strengths in the system that wouldn't be apparent under steady-state conditions [47], [48].

On the other hand, the power consumption profile of an annual simulation looks at longer-term, steady-state behavior, focusing on how the building interacts with the electrical grid over extended periods. This requires a different modeling approach, one that can aggregate or average out the minute-by-minute fluctuations to understand broader trends and impacts on energy consumption and production. Steady-state models often use hourly or daily data to provide insights into overall energy efficiency, seasonal variations, and long-term sustainability [49], [50]. These models are essential for strategic planning and policy development, as they help in predicting how changes in energy demand or supply might affect the grid over months or years [51]. Achieving a balance that meets the B2G system's simulation objectives within a reasonable computational time frame is a key challenge for system designers and engineers [52], [53]. All existing models of HVAC equipments like pumps, chiller and heatpump lack the integration of electrical component to simulate the effect of electrical grid parameters like sudden change in voltage and frequency conditions.

E. NOVELTY

To address these challenges, this work introduces a novel Computationally Efficient Aggregate Induction Machine (CEAIM) model that bridges the gap between high-fidelity transient simulation and scalable long-term energy modeling. Unlike conventional Motor Standard Library (MSL) or HVAC equipment models—which typically omit electrical dynamics or are too computationally intensive for grid-responsive scenarios—the proposed model integrates thermal, mechanical, and electrical domains within a single unified framework. This allows it to capture both fast transients (e.g., voltage/frequency disturbances) and long-term operational trends. The CEAIM model has been benchmarked to achieve a computational speedup exceeding 6000× compared to detailed MSL models, enabling large-scale or real-time simulation without compromising accuracy. Additionally, it is fully compatible with the Modelica-Buildings library, supporting direct integration into

building-to-grid (B2G) applications such as load shifting and frequency regulation.

III. MODEL DEVELOPMENT

As discussed in section II-D, none of the current models can meet the needs of B2G applications. Therefore, this paper introduces

- Computationally Efficient and Accurate Induction Machine (CEAIM) model
- HVAC Equipments coupled with CEAIM

The goal is to develop a model that meets the B2G system’s simulation objectives within a reasonable computational time frame. To achieve this goal, we propose to bypass the direct simulation of power electronic transitions, which is time consuming as most of the switching characteristic’s has low step size therefore huge number of equations required to be solved in a given time frame. Instead, we will substitute them with mathematical approximations based on physics based equations. This will reduce computing time, while conserving the details for B2G. It is worth to point out that this approach will ignore the losses, which is not critical for B2G application. These methods allow the model to compute the transient responses of voltage, current, and power consumption, completing an annual simulation within a few minutes. To develop this model, we will first use the physics based equations, then implement the model in Modelica, then proceed with a series of validations ranging from data-sheet to computational analysis.

A. VOLTAGE EQUATIONS IN DQ-AXIS

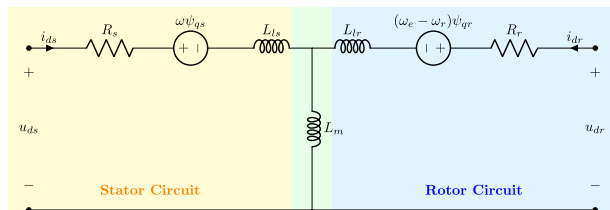


FIGURE 2. D-axis of the Induction Machine.

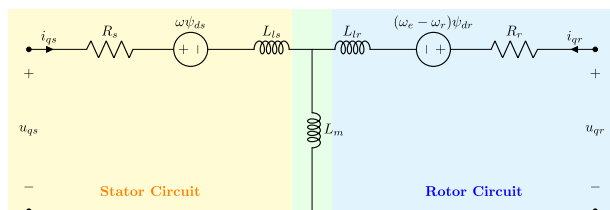


FIGURE 3. Q-axis of the Induction Machine.

The figures 2 and 3 represent the *D* and *Q* axis equivalent circuits of an induction machine in the rotating synchronous reference frame. The *Q*-axis circuit includes *Q*-axis stator voltage (u_{qs}), current (i_{qs}), stator resistance (R_s), induced voltage ($\omega\psi_{ds}$), and stator leakage inductance (L_{ls}). The rotor circuit includes *Q*-axis rotor voltage (u_{qr}), current

(i_{qr}), rotor resistance (R_r), induced voltage ($(\omega_e - \omega_r)\psi_{dr}$), and rotor leakage inductance (L_{lr}). The mutual inductance is L_m . The *D*-axis circuit similarly includes *D*-axis stator voltage (u_{ds}), current (i_{ds}), induced voltage ($\omega\psi_{qs}$), and *Q*-axis rotor voltage (u_{dr}), current (i_{dr}), with the same resistances and inductances. This approach decouples flux and torque components, simplifying analysis by highlighting the interaction between the stator and rotor in generating direct electromagnetic torque. The derivation of DQ based direct phase approach of induction machine is adapted from [54].

The stator equivalent voltage equations can be written as:

$$u_{ds} = R_s i_{ds} + \frac{d\Psi_{ds}}{dt} + \omega\Psi_{qs}, \quad (1)$$

$$u_{qs} = R_s i_{qs} + \frac{d\Psi_{qs}}{dt} + \omega\Psi_{ds}, \quad (2)$$

Equation 1 & 2 describe the *d*-axis and *q*-axis components of the stator voltage in a synchronous machine model. In these equations, u_{ds} and u_{qs} represent the *d*-axis and *q*-axis stator voltages, respectively. The term R_s denotes the stator resistance, while i_{ds} and i_{qs} are the *d*-axis and *q*-axis stator currents. The flux linkages in the *d*-axis and *q*-axis are represented by Ψ_{ds} and Ψ_{qs} , respectively. The electrical angular velocity is denoted by ω . These equations capture the dynamic behavior of the stator voltages by accounting for the resistive voltage drops, the time derivatives of the flux linkages, and the cross-coupling effects due to the machine’s rotation. Similarly, the rotor equivalent voltage equations can be written as:

$$u_{dr} = R_r i_{dr} + \frac{d\Psi_{dr}}{dt} - (\omega_e - \omega_r)\Psi_{qr}, \quad (3)$$

$$u_{qr} = R_r i_{qr} + \frac{d\Psi_{qr}}{dt} + (\omega_e - \omega_r)\Psi_{dr}, \quad (4)$$

Equation 3 & 4 describe the *d*-axis and *q*-axis components of the rotor voltage in a synchronous machine model. In these equations, u_{dr} and u_{qr} represent the *d*-axis and *q*-axis rotor voltages, respectively. The term R_r denotes the rotor resistance, while i_{dr} and i_{qr} are the *d*-axis and *q*-axis rotor currents. The flux linkages in the *d*-axis and *q*-axis are represented by Ψ_{dr} and Ψ_{qr} , respectively. The electrical angular velocity of the synchronous reference frame is denoted by ω_e , and the rotor’s angular velocity is denoted by ω_r . These equations account for the resistive voltage drops, the time derivatives of the flux linkages, and the effects of the relative motion between the electrical reference frame and the rotor.

B. FLUX EQUATIONS IN DQ-AXIS

The next step is to calculate the magnetic flux linkages of the stator and rotor, using the underlying equations:

$$\Psi_{ds} = (i_{ds}L_s + i_{dr}L_m), \quad (5)$$

$$\Psi_{qs} = (i_{qs}L_s + i_{qr}L_m), \quad (6)$$

$$\Psi_{dr} = (i_{dr}L_r + i_{ds}L_m), \quad (7)$$

$$\Psi_{qr} = (i_{qr}L_r + i_{qs}L_m), \quad (8)$$

Equation 5, 6, 7 & 8 describe the flux linkages in the d -axis and q -axis for both the stator and rotor in a synchronous machine. In these equations, Ψ_{ds} and Ψ_{qs} represent the d -axis and q -axis stator flux linkages, while Ψ_{dr} and Ψ_{qr} represent the d -axis and q -axis rotor flux linkages. The terms L_s and L_r denote the stator and rotor inductances, respectively, while L_m represents the mutual inductance between the stator and rotor. The variables i_{ds} and i_{qs} are the d -axis and q -axis stator currents, and i_{dr} and i_{qr} are the d -axis and q -axis rotor currents. These equations capture the interdependence of the flux linkages on the currents in both the stator and rotor, highlighting the coupled nature of the magnetic fields in the machine. The L_s and L_r can be written as:

$$L_s = L_{ls} + L_m, \quad (9)$$

$$L_r = L_{lr} + L_m, \quad (10)$$

C. ROTOR SPEED EQUATION AND ELECTROMAGNETIC TORQUE

Since induction machine is an electro-mechanical device, we can formulate the rotor speed based on the torque as

$$\omega_{rm} = \frac{P}{2J} \int (T_e - T_l) dt \quad (11)$$

align 11 represents the *mechanical angular velocity* ω_{rm} of the rotor shaft as a function of the net torque applied to the system in rad/s. In this equation, P is the total number of poles, and J is the moment of inertia of the rotor. The terms T_e and T_l denote the electromagnetic torque generated by the machine and the load torque, respectively. The integral $\int (T_e - T_l) dt$ captures the accumulation of net torque over time. The details for calculating the electromagnetic torques is shown as follows:

$$T_e = \frac{3P}{2} L_m (i_{qs} i_{dr} - i_{ds} i_{qr}). \quad (12)$$

D. CURRENT EQUATIONS FOR STATOR AND ROTOR IN DQ-AXIS

By substituting Equation (6) and Equation (5) into Equation (2) and Equation (1), the stator currents in d-q frames, namely i_{ds} and i_{qs} , can be expressed:

$$\frac{d}{dt} i_{ds} = \frac{1}{L_s} [u_{ds} - i_{ds} R_s - L_m \frac{d}{dt} i_{dr} + \omega_e L_s i_{qs} + \omega_e L_m i_{qr}]$$

and

$$\frac{d}{dt} i_{qs} = \frac{1}{L_s} [u_{qs} - i_{qs} R_s - L_m \frac{d}{dt} i_{qr} - \omega_e L_s i_{ds} - \omega_e L_m i_{dr}]. \quad (14)$$

By integrating the Equation (13) and Equation (14), the i_{ds} and i_{qs} are expressed as:

$$i_{ds} = \int \frac{1}{L_s} [u_{ds} - i_{ds} R_s - L_m \frac{d}{dt} i_{dr} + \omega_e L_s i_{qs} + \omega_e L_m i_{qr}] dt$$

and

$$i_{qs} = \int \frac{1}{L_s} [u_{qs} - i_{qs} R_s - L_m \frac{d}{dt} i_{qr} - \omega_e L_s i_{ds} - \omega_e L_m i_{dr}] dt. \quad (16)$$

Similarly, when the flux expressions are replaced in the voltage equations, the rotor currents i_{dr} and i_{qr} can be written as:

$$\frac{d}{dt} i_{dr} = \frac{1}{L_r} [u_{dr} - i_{dr} R_r - L_m \frac{d}{dt} i_{ds} + \omega_e L_r i_{qr} + \omega_e L_m i_{qs}]$$

and

$$\frac{d}{dt} i_{qr} = \frac{1}{L_r} [u_{qr} - i_{qr} R_r - L_m \frac{d}{dt} i_{qs} - \omega_e L_r i_{dr} - \omega_e L_m i_{ds}]. \quad (18)$$

After integration, they are described by Equations (19) and (20):

$$i_{dr} = \int \frac{1}{L_r} [u_{dr} - i_{dr} R_r - L_m \frac{d}{dt} i_{ds} + \omega_e L_r i_{qr} + \omega_e L_m i_{qs}] dt$$

and

$$i_{qr} = \int \frac{1}{L_r} [u_{qr} - i_{qr} R_r - L_m \frac{d}{dt} i_{qs} - \omega_e L_r i_{dr} - \omega_e L_m i_{ds}] dt. \quad (20)$$

IV. MODEL IMPLEMENTATION

A. CEAIM MODEL [55]

To evaluate the performance of CEAIM model, it is implemented in an equation-based object-oriented Modelica language [56]. Modelica has been used for building level energy modeling and simulations [57], [58], [59]. Implementing the model in Modelica allows it to be coupled with other existing Modelica models for B2G applications. In this paper, the models are compiled and simulated using Dymola 2023 [60], which is a Modelica environment.

Figure 4 shows the top level diagram of Modelica model. It contains four major parts: input variables, stator current, rotor current, and output variables. The input variables part provides the values of stator voltages, electrical and rotor frequency. The stator current part calculates di_{ds}/dt and di_{qs}/dt using Equations (13) and (14). The rotor current part calculates di_{dr}/dt and di_{qr}/dt using Equations (17) and (18). Third, the output variables provide the final values of the stator currents i_{ds} , i_{qs} using Equations (15) and (16) and rotor currents i_{dr} , i_{qr} using Equations (19) and (20).

1) IMPLEMENTATION OF CEAIM WITH VARIABLE FREQUENCY DRIVE

In B2G application, induction machine is often coupled with Variable Frequency Drive (VFD), which is modeled in this section. A VFD is a device used to control the speed of an electric motor. It operates by varying the frequency and voltage supplied to the motor. The process involves three stages: converting incoming AC power to DC, smoothing it in a DC intermediate stage, and then inverting it back to AC with variable frequency and voltage. This allows precise control of motor speed and torque. We propose a simplified model by not considering the internal operations and power electronics of the VFD (Figure 5 & 6) as the detailed power electronics switching characteristic's have low step size therefore huge number of equations required to be solved in a given time frame.

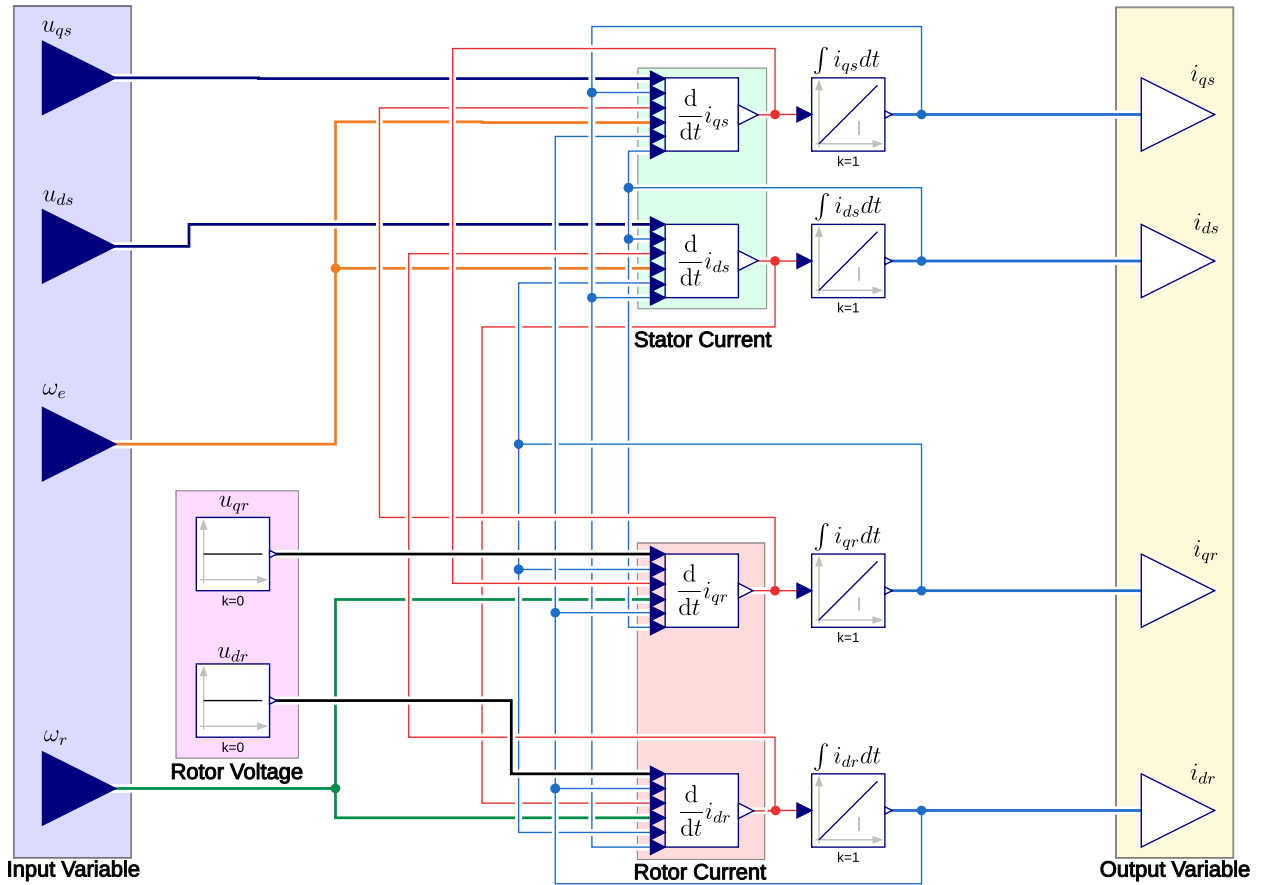


FIGURE 4. CEAIM model in Modelica.

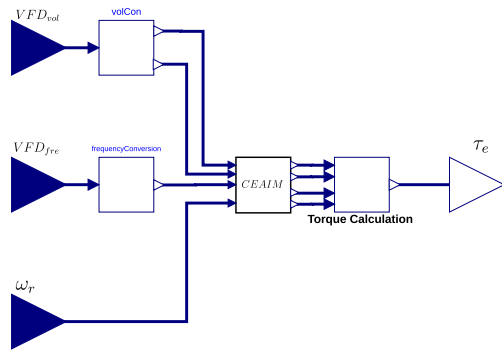


FIGURE 5. CEAIM model Machine interface.

Therefore we assume a constant V/F ratio to speed up the overall computational speed, where the VFD_{ratio} can be calculated by:

$$VFD_{ratio} = \frac{\text{Reference Speed [rev/min]}}{\text{Synchronous Speed of IM [rev/min]}} \quad (21)$$

Hence the updated voltage and frequency input to CEAIM can be formulated as in Equation (22) and Equation (23) respectively

$$VFD_{vol} = VFD_{ratio} \times u_{rms}, \quad (22)$$

$$VFD_{fre} = VFD_{ratio} \times f_{input}, \quad (23)$$

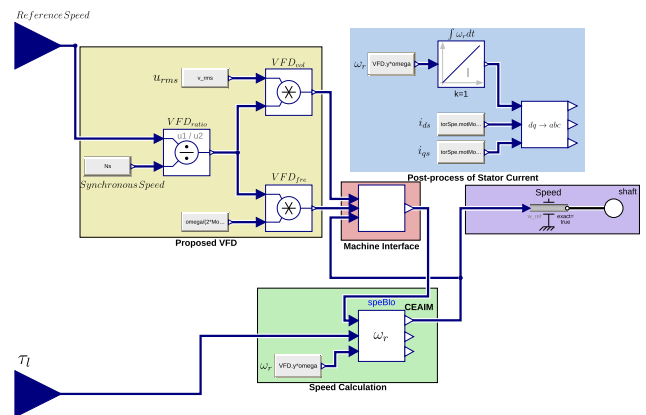


FIGURE 6. CEAIM combined with a variable frequency drive.

where VFD_{vol} is the adjusted input voltage to the induction machine, u_{rms} is the input voltage into the VFD, VFD_{fre} is the adjusted input frequency to the input machine and f_{input} is the reference frequency fed into the VFD.

B. CEAIM-HVAC

The proposed CEAIM-HVAC models are dependent on the existing chiller, heat pump and pump model available in Modelica Buildings Library (MBL) [61], a widely used open-source platform for simulating building energy and

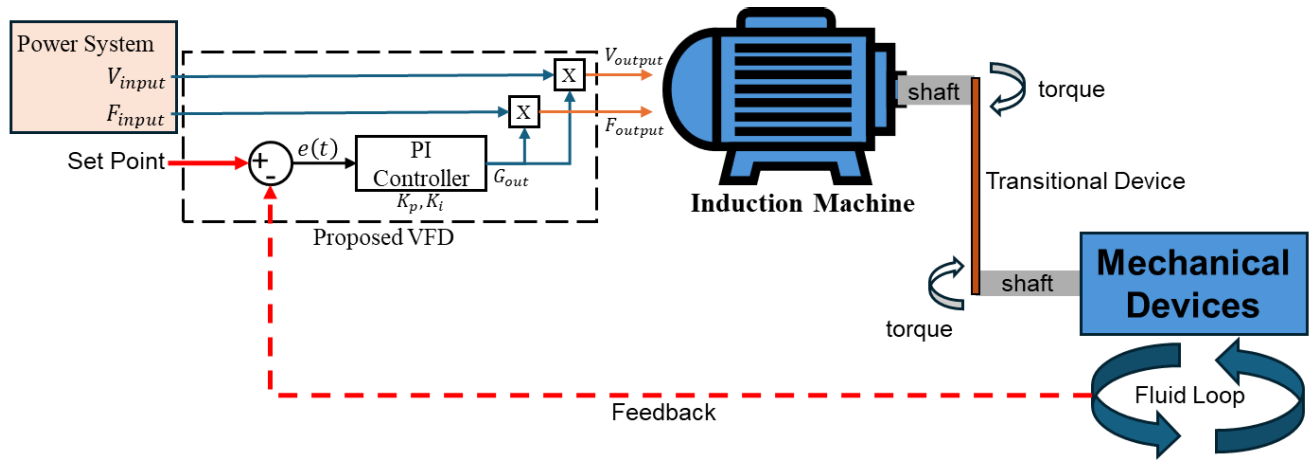


FIGURE 7. Implementation of CEAIM - HVAC.

HVAC systems. The proposed models are designed to be integrated as a dedicated package within the MBL as “Motor-Drive”. This integration will enhance the library’s capability to model grid-interactive building systems, enabling researchers and practitioners to evaluate energy performance, analyze grid responsiveness, and develop advanced control strategies with ease.

The proposed model (Figure 7) receives voltage and frequency signal from power system and the user will be able to provide a set point for the chiller, heat pump and pump as required, due to its robust feedback loop the model adapts to the sudden changes in the signals (Table 2).

TABLE 2. Operating conditions of CEAIM-HVAC equipments.

Model	Setpoint/Feedback	Units
CEAIM-Pump	Flow Rate	[kg/s]
CEAIM-Heat Pump	Temperature	[K]
CEAIM-Chiller	Temperature	[K]

V. MODEL VALIDATION

To systematically validate the CEAIM model, we perform a top-down approach starting from a steady state performance to a full dynamic process. First, we compare the CEAIM model with datasheet values at steady state by considering only the nominal operating conditions. Second, we compare the performance of CEAIM under various steady state operating conditions with the operational curves available in the market. Third, we extend the comparison to a dynamic startup sequence with an existing hardware setup to evaluate CEAIM’s performance in transient conditions. Fourth, CEAIM undergoes VFD operations testing under various frequency settings. This is crucial for applications requiring speed control and energy efficiency.

A. STEADY-STATE VALIDATION AT NOMINAL CONDITIONS

The section validates the CEAIM model under the deviations of speed and power factor in steady state conditions for a wide rating of IMs from the ABB Handbook [62]. Table 3 shows the efficiency and power factor comparisons for five

different IMs with rating power from 4 kW to 75 kW. The simulation results have demonstrated that the CEAIM can predict efficiency and power factor with a relative error below 3% (Table 3).

B. STEADY-STATE COMPARISON UNDER OFF-DESIGN CONDITIONS

The previous step validates the performance of CEAIM for five different motors under nominal conditions. This section validates the off-design performance of the CEAIM. In this case, the parameters of ABB MBT112M, with a capacity of 4 kW, are used for setting up the CEAIM model. The details of the parameters are listed in Table 4.

Due to the unavailability of data for the ABB MBT112M in terms of efficiency, power factor (PF), current, and slip under different off-design conditions, we used data from a similar model, W22IE3112M, with the same rated power of 4 kW [63]. It should be noted that the performance curves will be different in the comparison. However, the objective is to check if the CEAIM can capture a similar trend of performance curves at off-design conditions. Thus, the differences in the performance curves are acceptable.

Figure 8 illustrates the comparison results regarding the efficiency, power factor (PF), current, and slip under different percentages of the rated output. These operational curves are crucial as they depict how the machine’s performance varies under different loading conditions. In general, the CEAIM model can capture the trends of the four key variables except there are some discrepancies for slip and efficiency when the rated output is larger than 60%. The reason is that the efficiency of IM largely depends on the material and construction of the winding which varies amongst vendors.

C. TRANSIENT BEHAVIOR VALIDATION

The previous two sections validate the CEAIM’s performance in steady state conditions. This section is to validate its performance in transient condition. The transient conditions refer to the machine’s response to changes in its operational

TABLE 3. Comparison of simulated results with ABB Handbook [62].

Model	Rating [kW]	Efficiency [%]			Power Factor		
		CEAIM Model	Datasheet	Error [%]	CEAIM Model	Datasheet	Error [%]
M2QA112M4A	4	84.46	84.50	-0.05	0.83	0.84	-1.67
M2QA112M4A3GQA112301	4	84.8	85.00	-0.24	0.80	0.82	-2.44
M2QA132M4A3GQA132301	7.5	85.89	88.50	-2.95	0.86	0.85	1.53
M2QA200L4B3GQA202502	37	89.14	89.20	-0.07	0.87	0.88	-1.59
M2QA250M4B3GQA252302	75	89.65	90.40	-0.83	0.89	0.87	1.77

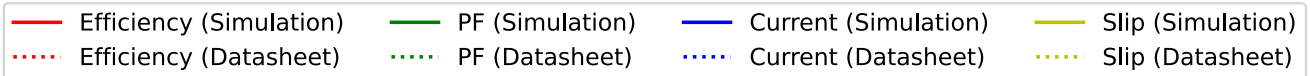
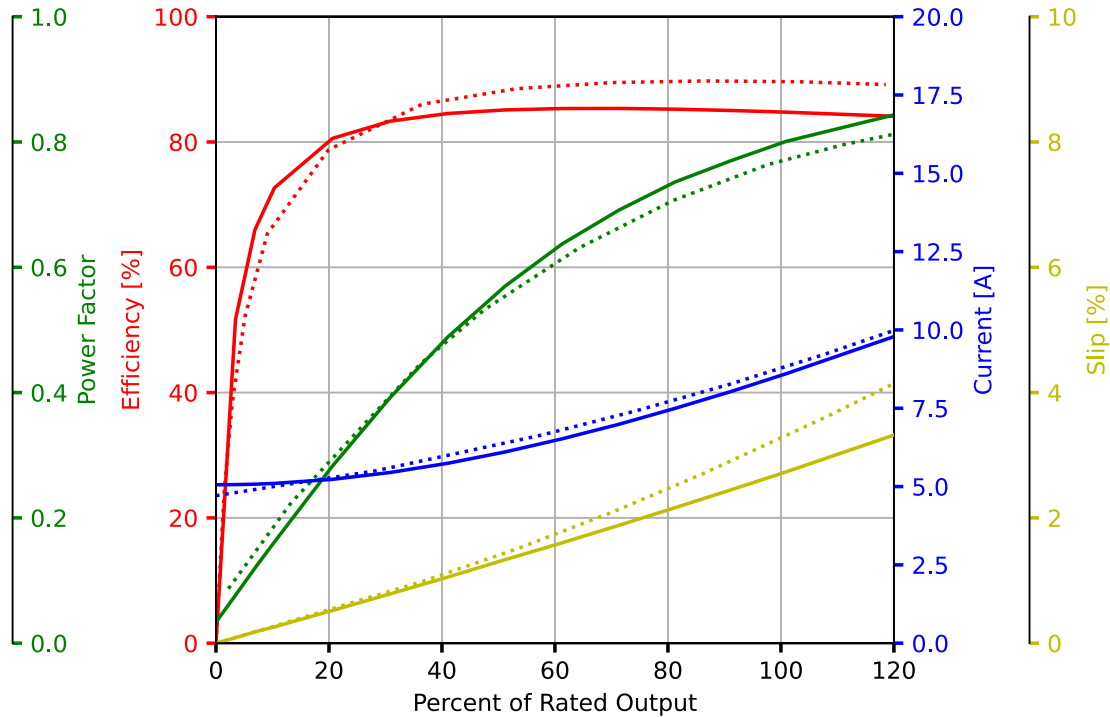


FIGURE 8. Proposed model vs. similar sized induction machine in market.

TABLE 4. Rated specifications and simulation parameters of the asynchronous induction motor (ABB MBT112M).

Parameters	Value	Unit
Rated Power	4	[kW]
Rated Voltage	400	[V]
Rated Frequency	50	[Hz]
Rated Speed	1442	[RPM]
Rated Current	8.62	[A]
Stator Resistance	1	[Ω]
Rotor Resistance	1.145	[Ω]
Stator Inductance	0.1457	[H]
Rotor Inductance	0.1458	[H]
Mutual Inductance	0.1406	[H]
Moment of Inertia	0.051	[kg m ²]
Total Inertia	0.17	[kg m ²]
Load Torque	26.5	[Nm]
Poles	4	

state, such as start-up, shutdown, or sudden changes in load. Here the performance of the CEAIM during a start-up period

is studied. To ensure consistency with the model used in [64], the induction motor model adopted in this study also neglects iron losses and magnetic saturation. This simplification is appropriate, as the primary objective is to compare dynamic behavior under equivalent modeling assumptions. Figure 9 shows that the performance of our model in comparison with the simulated setup described in [64]. The close agreement between the simulation results presented here and those in [64] can be attributed to the use of fundamentally similar models, which exclude the same secondary effects. The variables, such as rotor speed, torque, electrical current, and overall power consumption, are presented to evaluate the CEAIM model’s performance and reliability against an already established model.

First, Figure 9a provides a plot of rotor speed response. It shows that the CEAIM model is able to simulate the non linear start-up condition with very high accuracy. Second, Figure 9b provides a plot of electromagnetic torque response

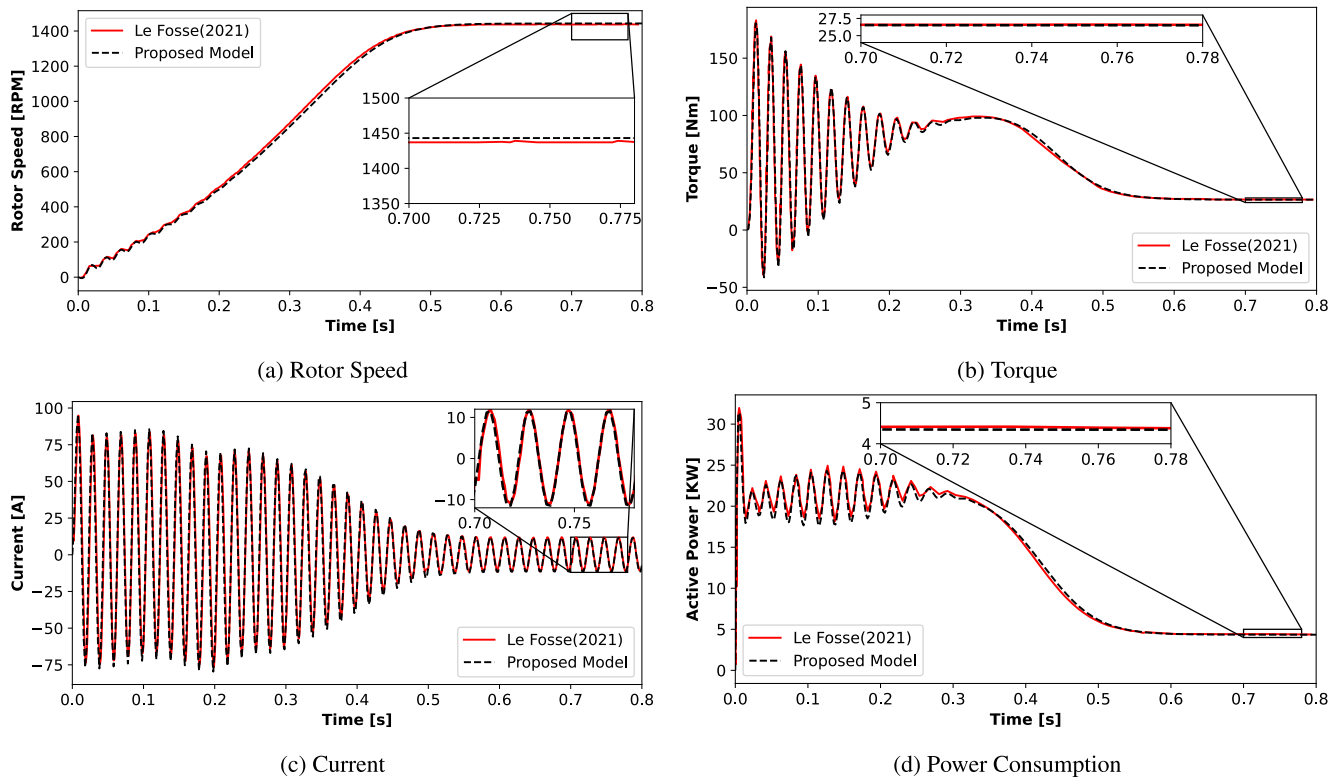


FIGURE 9. Simulation results: proposed model vs. reference model from [64] (iron losses and saturation neglected).

with high level of accuracy. Third, Figure 9c provides a plot of input current. CEAIM model is able to capture the transients condition of input current as the starting current is approximately 8 times higher than the steady state condition. Once IM reaches the nominal operating condition, input current fall down to a periodic sine wave with magnitude of 10A. Fourth, Figure 9d illustrates the variations of active power consumption and indicates that the CEAIM can achieve high accuracy in estimating the active power consumption at both the start-up and steady-state periods.

Upon validation of the startup sequence, we extended the simulation to study the characteristic of CEAIM in varied load ranges. The model was subject to a load variation of 20% above and below the rated load (Figure 10). As shown in the simulated power consumption profiles, the model responds consistently across these conditions, capturing both the transient startup phase and steady-state power behavior. Although no experimental data was available for these specific load levels, the simulation results suggest that the CEAIM model maintains dynamic fidelity and numerical stability across a range of operating points, making it suitable for applications involving load variation.

D. TRANSIENT BEHAVIOR COMPARISON UNDER VARIABLE FREQUENCY DRIVE CONTROL

In B2G application, IM is often coupled with Varying Frequency Drive (VFD). Hence, the primary aim of adding

the VFD to our proposed model was to simulate and study the response of the system under different speed control signals. This section evaluates three types of input signals: ramp, step, and pulse. It is noted that the parameters of setting up the CEAIM model and the reference results are obtained from [65]. It is important to note that the reference study employs PI controllers to regulate the VFD. However, this study uses the VFD_{ratio} to manage changes, as shown in Figure 6, resulting in minor differences in results.

Figure 11 compares the simulation results from the CEAIM model and the reference results from [65] under various control signals. Figure 11a illustrates the response of the CEAIM model to the ramp signals. The control signals gradually change from -100 rad/s to 100 rad/s, remain steady at 100 rad/s for a while, and slowly return to -100 rad/s. It can be observed that both simulation and reference results can accurately follow the ramp signals. Figure 11b represents the IM's reaction to an abrupt signal change. The CEAIM model responds quickly, reaching a steady state with fewer oscillations compared with the reference results. Figure 11c showcases the response of the IMs to pulse signals fluctuating between -30 and $+30$. The outcomes from the CEAIM model align with the reference data, despite the CEAIM model having more oscillation. The differences observed from Figures 11b and Figure 11c can be explained by the existence of the PI controller in this study. Though there are minor differences, the results can still demonstrate that the

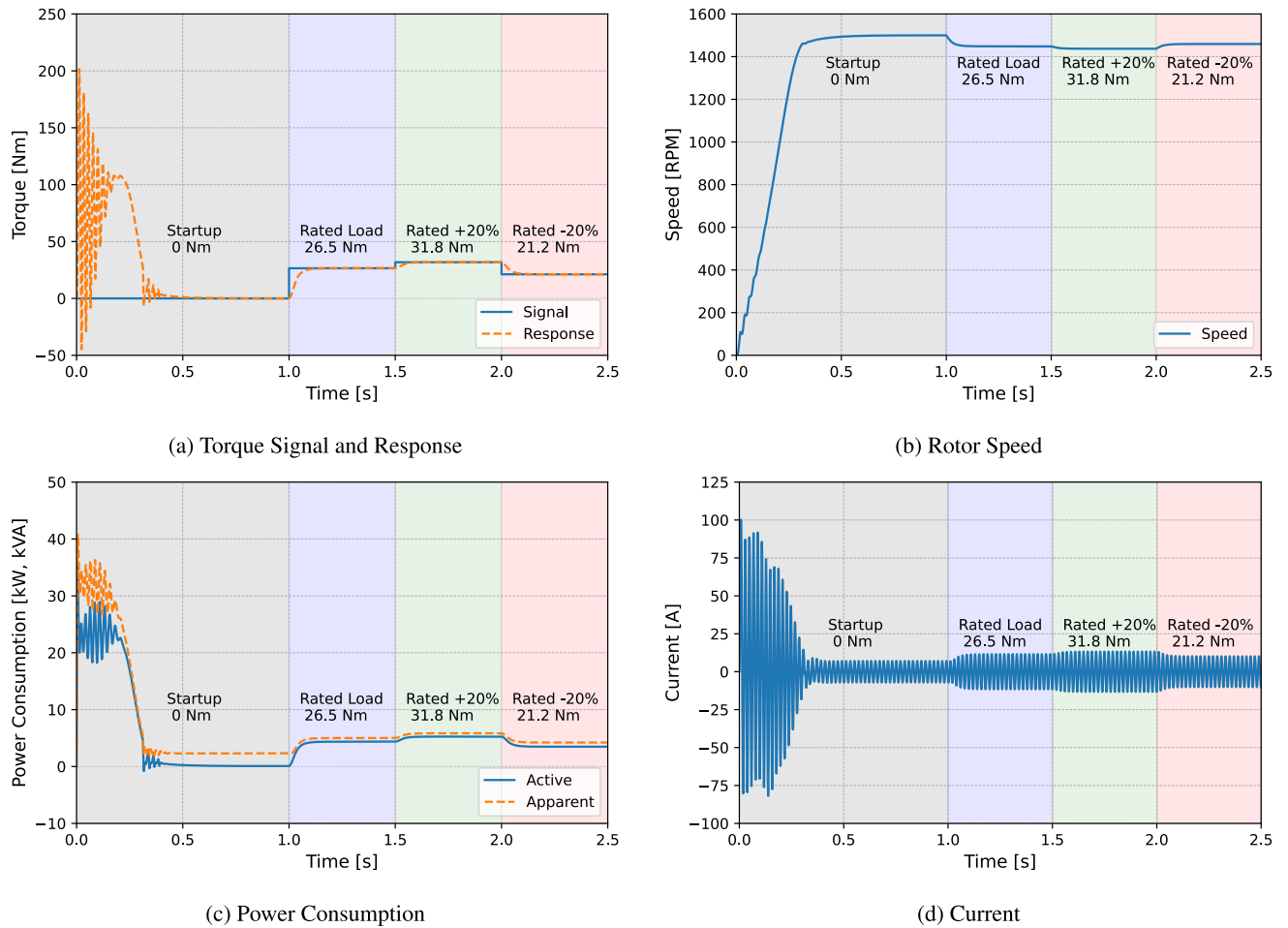


FIGURE 10. CEAIM - load variation.

TABLE 5. Overall comparison of MSL vs CEAIM model.

Category	MSL	CEAIM
Modeling technique	Space phasor transformation	dq0
Equilibrium points	Yes	Yes
Small-signal	Yes	Yes
Transients	No	Yes
Assumptions	Relatively slow variation in amplitude	Fast variation in amplitude
Approximations	The voltage and current are near sinusoidal	Nil
System dynamics	Quasi-static model	Transient model

CEAIM model, equipped with a VFD, can effectively capture the operational dynamics of an induction machine.

The dynamic behavior of the proposed CEAIM model was evaluated under variable frequency excitation ranging from 10 Hz to 50 Hz, and the corresponding simulation results for torque, current, power, and speed were analyzed. As expected, the rotational speed of the machine increases proportionally with frequency, closely following the theoretical synchronous speed limit defined by $N_s = \frac{120 \cdot f}{P}$, where f is the supply frequency and P is the number of poles.

This agreement between simulation and theory indicates that the model accurately captures the electrical-mechanical coupling inherent in induction machines. Similarly, the variations in current and power consumption reflect the increased mechanical loading and energy demand at higher frequencies. While *no experimental measurements were available* for validation, the consistency of these responses with theoretical expectations provides confidence in the model’s fidelity under frequency-varying scenarios. (Figure 12)

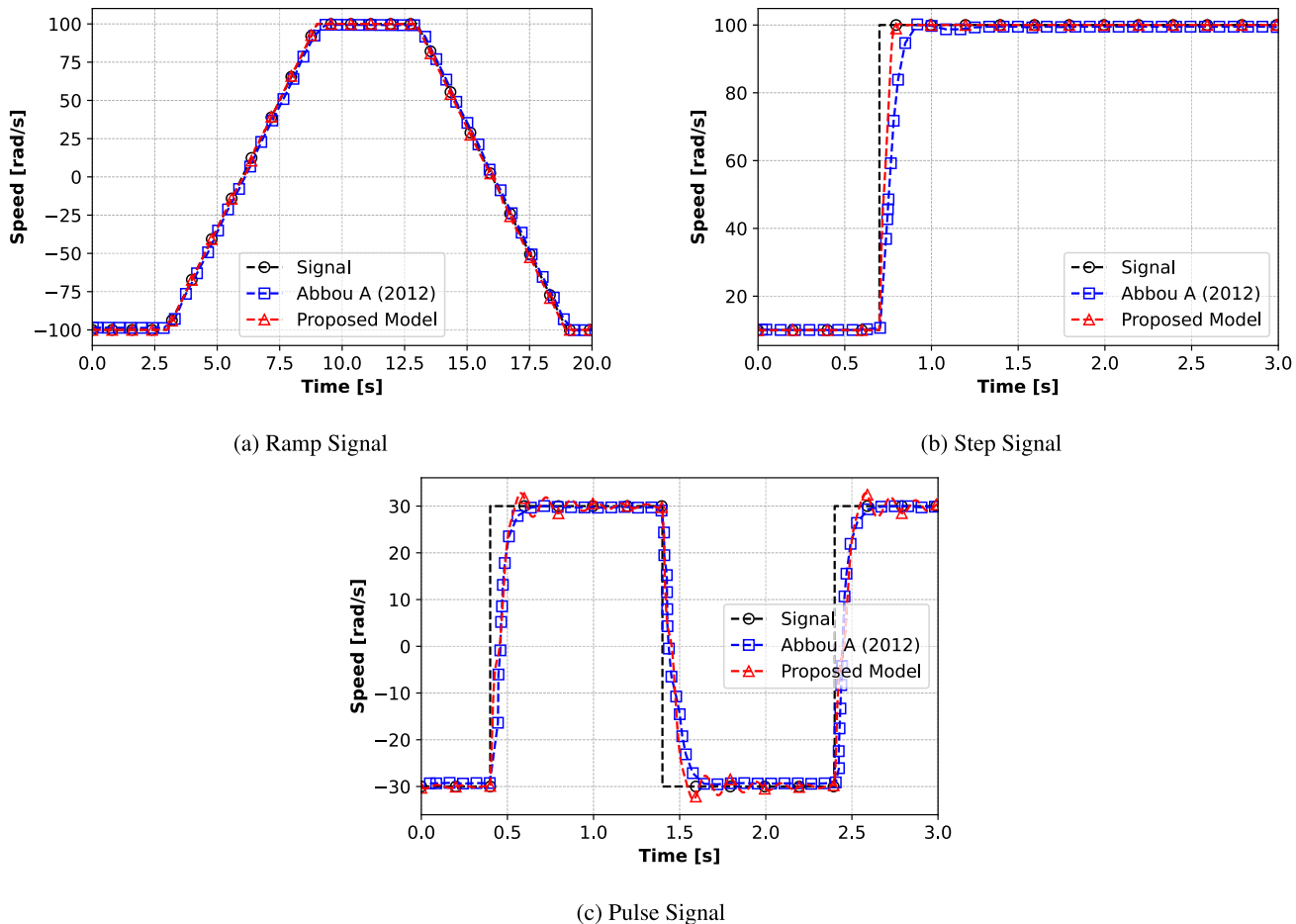


FIGURE 11. System response of CEAIM combined with a variable frequency drive.

VI. CROSS COMPARISON WITH MODELICA STANDARD LIBRARY

A. ACCURACY AND ERROR CALCULATION

We compare the proposed CEAIM model with an induction machine model from the Modelica Standard Library (MSL) [56], a well-established and widely used resource for system simulation. The MSL model employed in this study is designed with a quasi-steady-state formulation (Table 5), making it suitable for steady-state or slowly varying conditions. In contrast, the CEAIM model is developed with the explicit capability to simulate transient dynamics, particularly relevant for integrated building-to-grid (B2G) simulations. This comparison is not intended as a direct one-to-one evaluation of modeling fidelity but serves to demonstrate the extended transient modeling capability of the CEAIM model. For this purpose, we evaluate both models using a third, validated reference model [64] as a baseline. Key performance variables selected for analysis include rotor speed response, torque, and power consumption, as these are critical indicators of induction machine behavior under both dynamic and steady-state conditions.

The comparative results are illustrated in Figure 13, highlighting how each model responds across these variables.

As expected, significant differences appear during transient conditions due to the differing modeling approaches: the MSL model assumes quasi-steady-state behavior, whereas the proposed model is fully transient-capable. These differences are quantified using standard statistical metrics, including the coefficient of variation of the root mean square error (CVRMSE), normalized mean bias error (NMBE), and coefficient of determination (R^2).

$$CV\ RMSE[\%] = \frac{1}{\bar{m}} \cdot \sqrt{\sum_{i=1}^n \frac{(m_i - s_i)^2}{n}} \times 100, \quad (24)$$

$$NMBE[\%] = \frac{1}{\bar{m}} \cdot \sum_{i=1}^n \frac{(m_i - s_i)}{n} \times 100, \quad (25)$$

$$R^2 = \left(\frac{n \cdot \sum_{i=1}^n m_i \cdot s_i - \sum_{i=1}^n m_i \cdot \sum_{i=1}^n s_i}{\sqrt{(n \cdot \sum_{i=1}^n m_i^2 - (\sum_{i=1}^n m_i)^2) \cdot (n \cdot \sum_{i=1}^n s_i^2 - (\sum_{i=1}^n s_i)^2)}} \right)^2, \quad (26)$$

where m_i , s_i and \bar{m} are the measured value, simulated value, and mean of the measured value respectively for n number of observations.

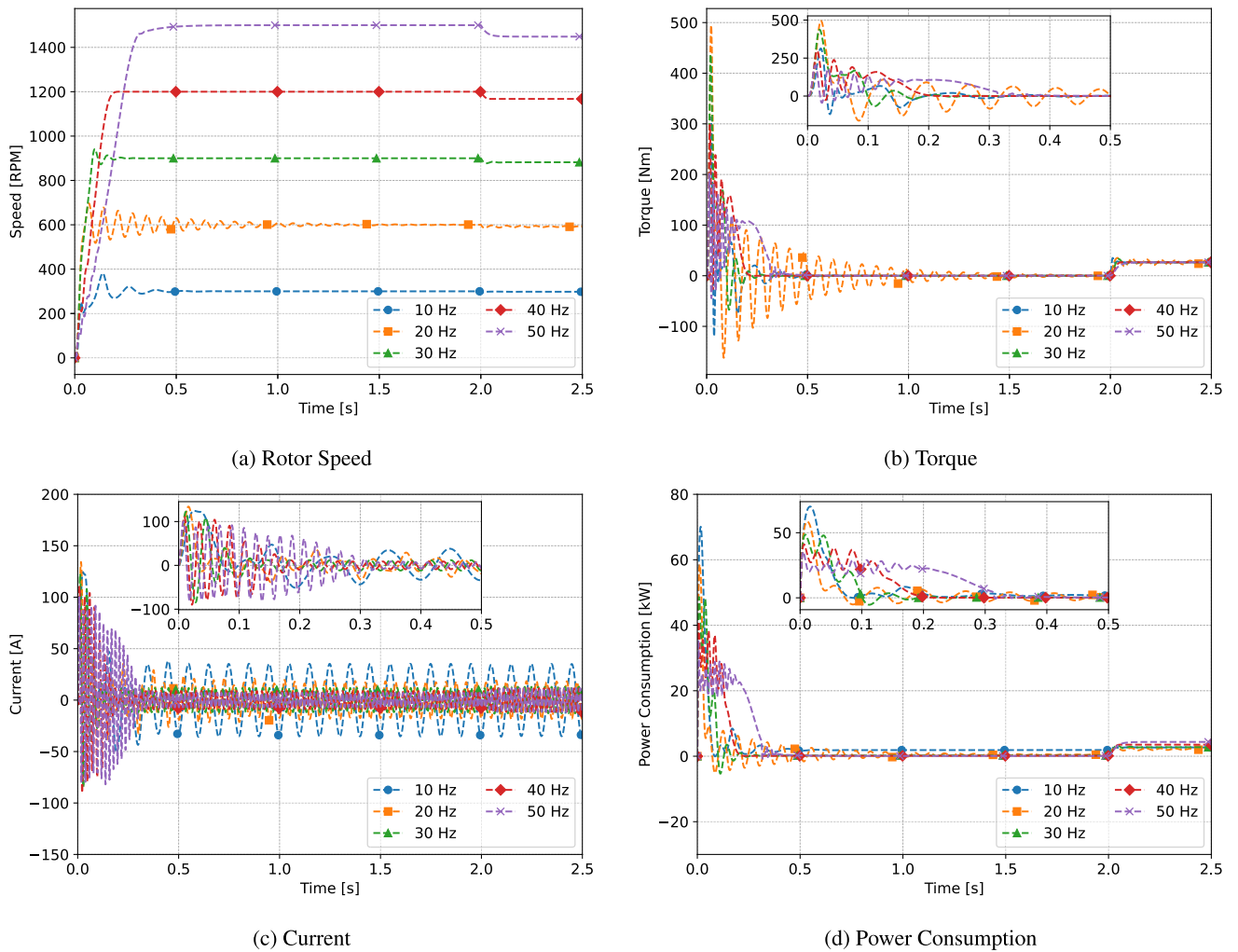


FIGURE 12. CEAIM - frequency variation.

TABLE 6. Summary of CVRMSE.

Simulation Period	Model	CV (RMSE) [%]		
		Torque	Speed	Power
Transient	MSL	89.28	66.09	67.60
	PROPOSED	6.44	2.12	3.08
Steady State	MSL	4.75	0.16	11.25
	PROPOSED	0.48	0.27	2.04
Full Simulation	MSL	92.05	32.11	72.11
	PROPOSED	6.67	0.61	3.16

The error and accuracy are calculated based on the Direct On Line (DOL) startup of the induction motor as depicted in Figure 13. A total of 160 data points at every 0.005 second were considered for the full simulation in which first 110 points contribute to the transient period and the remaining 50 points contribute to the steady state period. Table 6 shows a comprehensive summary of the CVRMSE calculated using Equation (24). Table 7 presents a comprehensive summary of NMBE calculated using Equation (25). Table 8 provides a comprehensive summary of R² calculated using Equation (26). According to the three tables, the MSL model performs well in estimating the steady-state results

but significantly underperforms in predicting the transient behaviors of IM. On the other hand, the proposed model (CEAIM) can accurately capture both transient and steady-state behaviors.

TABLE 7. Summary of NMBE.

Simulation Period	Model	NMBE [%]		
		Torque	Speed	Power
Transient	MSL	6.82	-53.31	60.14
	PROPOSED	1.15	1.15	1.06
Steady State	MSL	4.74	0.12	11.16
	PROPOSED	0.02	-0.26	1.01
Full Simulation	MSL	6.55	-18	56.10
	PROPOSED	0.99	-0.1	1.06

These results confirm the CEAIM model’s ability to accurately capture both transient and steady-state behavior, supporting its suitability for B2G applications that require detailed dynamic response.

B. LARGE-SCALE SYSTEM SCALABILITY

To further illustrate the capabilities of CEAIM model, we considered a large scale system modeling to compare the

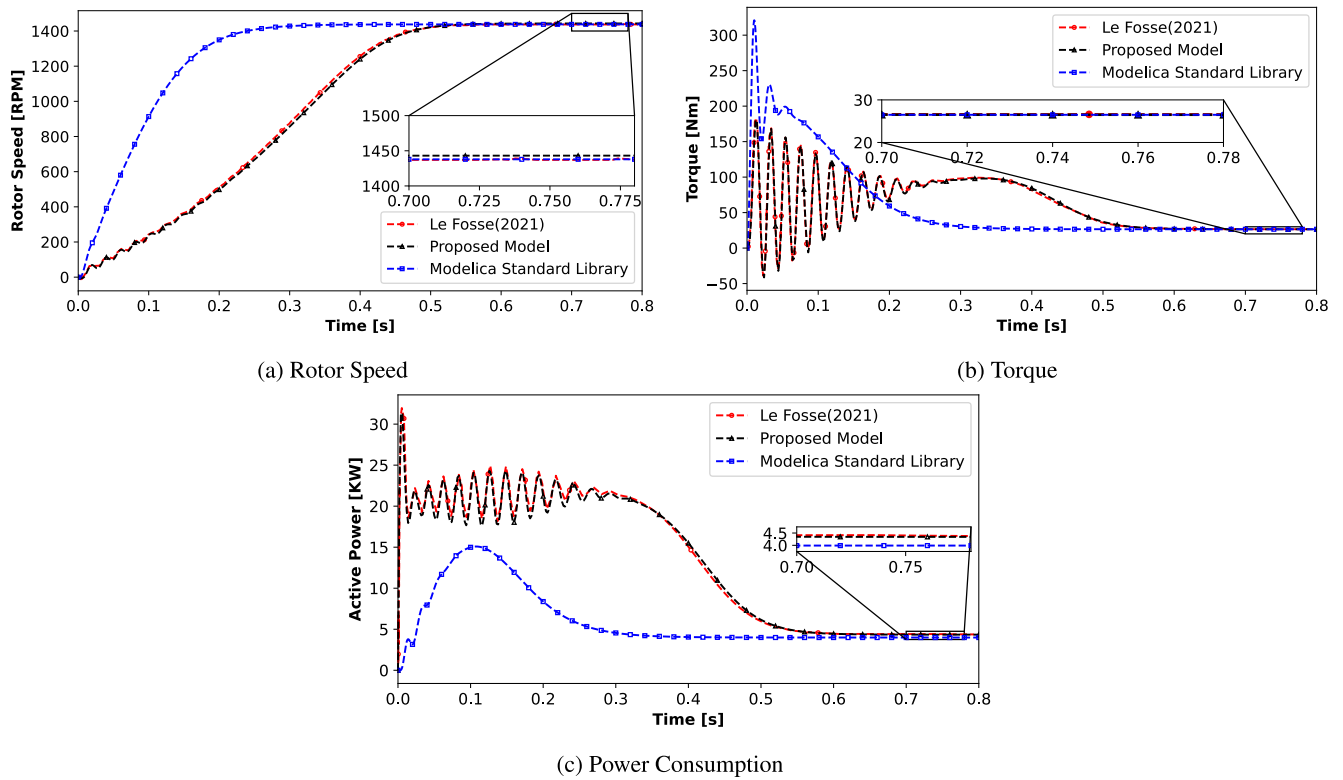


FIGURE 13. Modelica standard library vs proposed model.

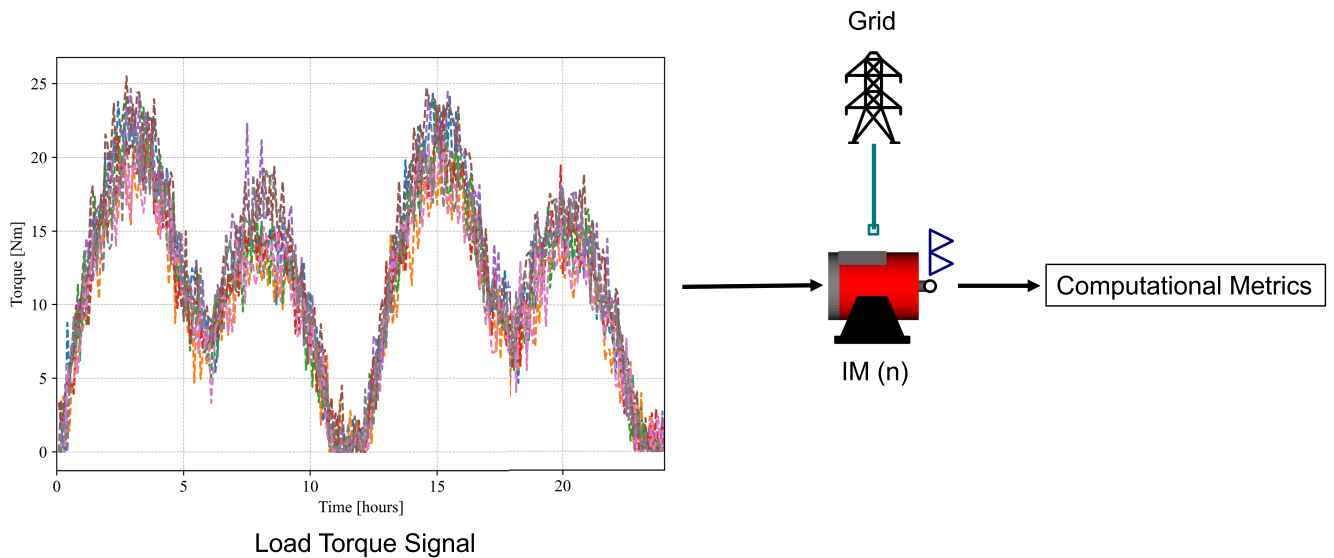


FIGURE 14. Large scale modeling simulation setup.

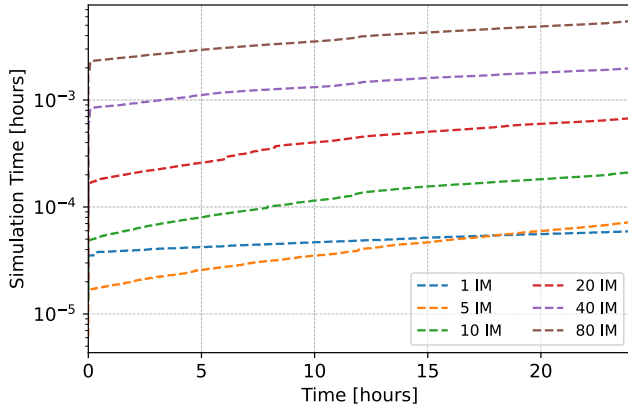
computational capability alongside the MSL model. It is to be noted that this study considers the example IMC_DOL from the MSL. The study included a 24 hour simulation profile with similar load torque to both the CEAIM and MSL systems (Figure 14). The simulation results (Figure 15) shows the overall simulation time taken by the respective models, in terms of computational speed, the proposed CEAIM model stands out for its remarkable efficiency. Upon calculation of

Big-O notation:

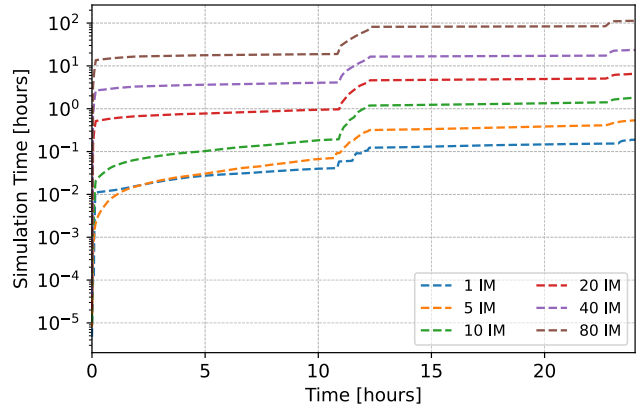
$$CEAIM(s) \rightarrow 0.073 \times n^{1.28}$$

$$MSL(s) \rightarrow 680 \times n^{1.46}$$

The given expressions show how two quantities, $CEAIM(s)$ and $MSL(s)$, scale with the problem size n . Specifically, $CEAIM$ grows approximately as $0.073 \times n^{1.28}$, and MSL grows as $680 \times n^{1.46}$. In Big-O notation, this means



(a) CEAIM



(b) MSL

FIGURE 15. Large scale modeling system response.

TABLE 8. Summary of R².

Simulation Period	Model	R ²		
		Torque	Speed	Power
Transient	MSL	0.01	0.62	0.25
	PROPOSED	0.98	1	0.99
Steady State	MSL	1	1	0.85
	PROPOSED	1	0.99	1
Full Simulation	MSL	0.0824	0.63	0.34
	PROPOSED	0.987	0.99	0.99

$CEAIM = O(n^{1.28})$ and $MSL = O(n^{1.46})$. The exponents indicate that both grow faster than linearly but slower than quadratically, with MSL growing noticeably faster than $CEAIM$ as n increases. Although MSL starts with a much larger constant (680 vs. 0.073), making it initially much larger, the critical point is that $CEAIM$ is asymptotically faster for larger simulations because its growth rate with respect to n is lower. As n becomes large, the difference in growth rates (1.28 vs. 1.46) becomes increasingly important, meaning $CEAIM$ will outperform MSL more and more as the simulation size scales up.

In comparing model size and complexity (Table 9 and Table 10), MSL is significantly larger than $CEAIM$, featuring roughly twice as many unknowns and equations. MSL also introduces substantially more aliasing (340 versus 135 alias variables), indicating a more interconnected structure that can negatively impact solver performance. From the perspective of linear system complexity, $CEAIM$ is simpler, involving only a small 2×2 linear system, whereas MSL contains multiple linear systems of sizes $\{3, 14, 2\}$, with residual complexities even after system manipulation ($\{0, 4, 0, 2\}$). This added complexity suggests that MSL is considerably more computationally demanding. Given these differences, $CEAIM$ is more efficient for simulation: it has fewer unknowns, smaller and simpler linear systems, fewer alias variables, and a leaner overall equation structure. In contrast, MSL 's larger system size and higher aliasing, even without

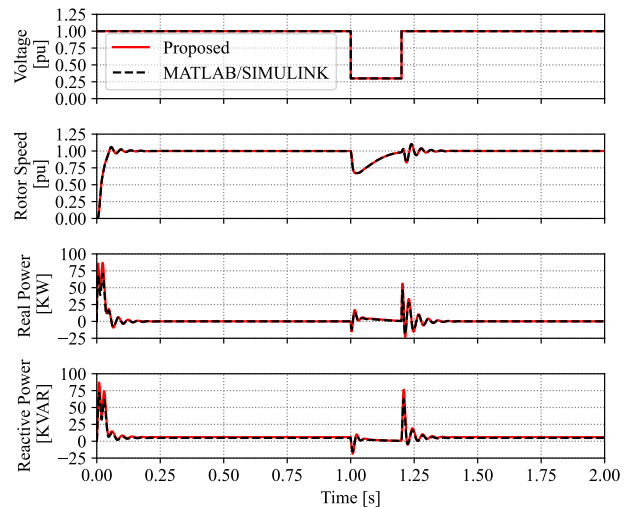


FIGURE 16. Grid interaction: CEAIM.

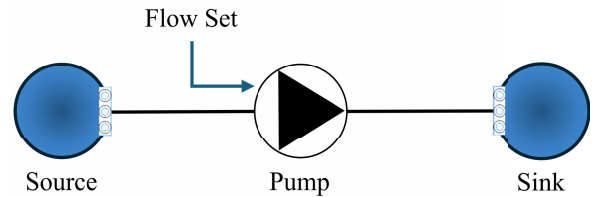


FIGURE 17. Test setup: Pump.

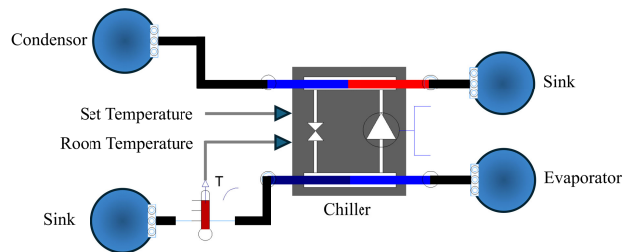


FIGURE 18. Test setup: Chiller.

nonlinear systems, likely result in longer model translation and simulation times.

TABLE 9. Translation Metric 1 IM.

Metric	CEAIM	MSL
Components	65	68
Variables	380	751
Parameters	168 (3353 scalars)	278 (3513 scalars)
Unknowns	211 (229 scalars)	461 (535 scalars)
Differentiated Vars	9	23
Equations (Total)	216	294
Non Trivial Equations	190	229
Constants (Translated)	83	237
Free Parameters	3221	3215
Parameter-Dependent	78	158
Time Varying Vars	66	110
Alias Variables	135	340
Continuous States	8	7
Linear Systems	{2,2}	{3,14,2}
Nonlinear Systems	0	0
Numerical Jacobians	0	0

TABLE 10. Simulation Metric 1 IM.

Metric	CEAIM	MSL
CPU-time for integration (s)	0.073	680
CPU-time for one grid interval (ms)	0.146	1.36e3
CPU-time for initialization (s)	0	0
Number of result points	1105	1073
Number of grid points	501	501
Number of accepted steps	10456	35632357
Number of f-evaluations (dynamics)	20919	92660856
Number of crossing function evaluations	11369	35704015
Number of Jacobian-evaluations	4844	21332363
Number of model time events	289	289
Number of input time events	0	0
Number of state events	15	0
Number of step events	0	0
Minimum integration stepsize	3.17e-11	4.1e-5
Maximum integration stepsize	147	2.58
Maximum integration order	5	5

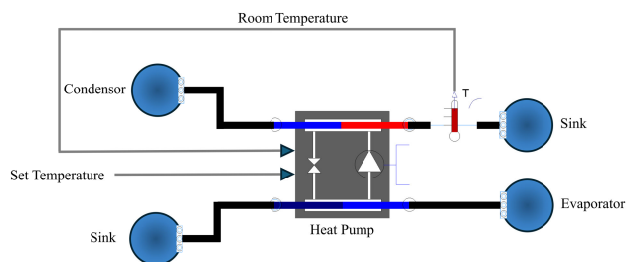


FIGURE 19. Test setup: Heat pump.

It is also worth mentioning the performance improvements refer to system-level modeling scenarios, not to detailed electromagnetic transient simulations. Tools such as PSCAD or EMTD are highly specialized for fine-grained EMT analysis, which is outside the scope and intended application of the proposed CEAIM model. Our model is designed for multi-domain, scalable, and fast simulations within frameworks like Modelica, where integrating electrical, mechanical, thermal, and fluid dynamics is essential. While the proposed model demonstrates significantly faster simulation performance compared to the MSL model, this difference reflects a divergence in modeling objectives rather than a critique of MSL. The MSL models are designed for detailed electrical engineering analysis and include complex phenomena such as power electronic switching. These features are essential

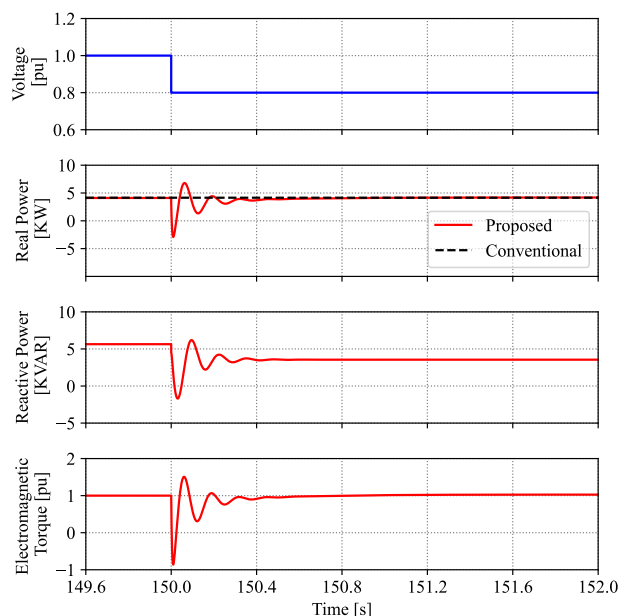


FIGURE 20. Grid interaction: Pump.

for high-fidelity component-level simulations but come with increased computational demands. In contrast, our model intentionally abstracts away such details to achieve a balanced level of representation that is computationally

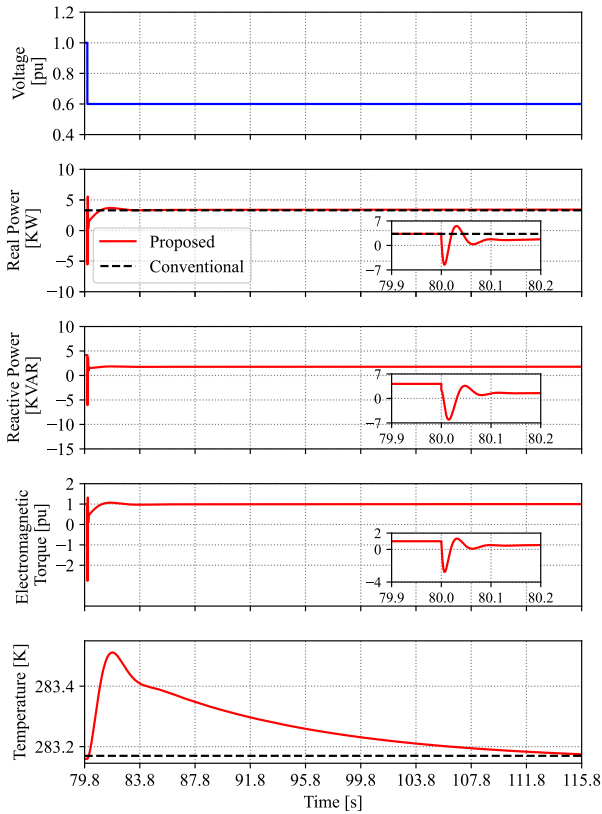


FIGURE 21. Grid interaction: Chiller.

efficient and well-suited for system-level co-simulation. This design enables interoperability with other domains, such as HVAC systems including chillers, heat pumps, and pumps making the model especially useful for integrated building energy simulations. Thus, the proposed model is intended to complement, not replace, existing MSL models by addressing use cases where speed and cross-domain coupling are prioritized over fine-grained electrical detail.

VII. CASE STUDY: GRID INTERACTION

This study presents a simulation-based analysis of electrical grid dynamics in the context of CEAIM and CEAIM-HVAC equipments. The case study is designed to model the interaction of these systems with the power grid, focusing on operational behavior under varying electrical grid conditions.

To analyze the influence of the electrical grid on various systems, a series of case studies were conducted, subjecting an induction machine (CEAIM) (Figure 16), pump (CEAIM-pump) (Figure 17), chiller (CEAIM-Chiller) (Figure 18) and heat pump (CEAIM-Heat Pump) (Figure 19) to sudden changes in load voltage. This scenario help to evaluate the transient and steady-state behavior, focusing on key aspects such as voltage stability, electromagnetic torque fluctuations, and system-specific responses, including mass flow rate heating and cooling performance. To provide a meaningful comparison, the developed models were tested alongside a conventional model from MATLAB

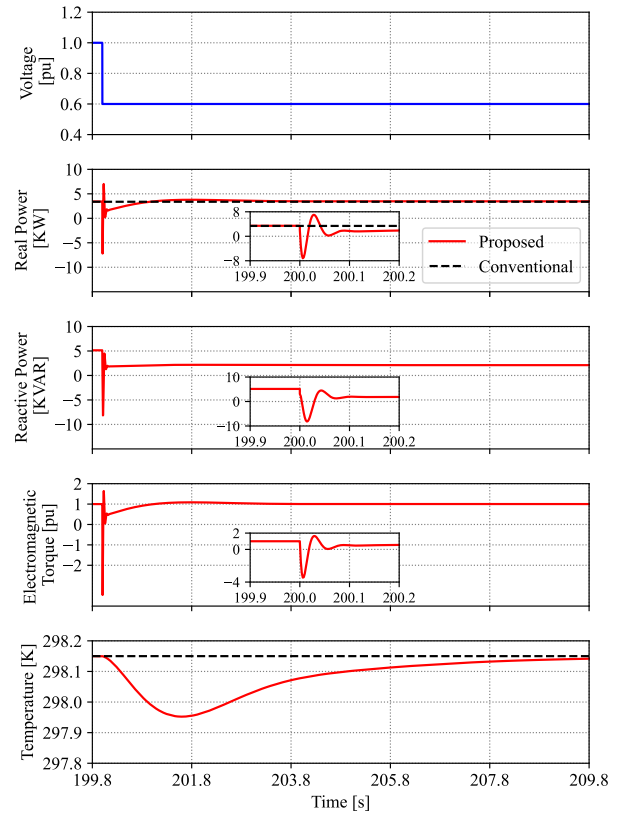


FIGURE 22. Grid interaction: Heat pump.

Simulink for Induction Machine and MBL models such as (Buildings.Fluid.Movers.FlowControlled_m_flow), (Buildings.Fluid.Chillers.CarnotTEva) and (Buildings.Fluid.HeatPumps.EquationFitReversible) under identical conditions.

This comparison demonstrates that the proposed CEAIM model is fully capable of simulating both transient and steady-state conditions. The validation against the MATLAB/Simulink model shows a strong agreement in key system responses, including rotor speed, active power, and reactive power dynamics at sudden voltage variations (Figure 16).

The results (Figures 20, 21, 22) clearly show that the proposed model is designed for dynamic system operation, allowing it to respond effectively to voltage changes. It can manage transient conditions by dynamically adjusting active power, reactive power, and electromagnetic torque. In contrast, the conventional model is limited to steady-state operation and lacks the ability to react or provide meaningful calculations for transient parameters like reactive power and torque.

The key point to observe in Figure 21 and Figure 22 is that there is a significant difference in the electrical domain (active and reactive power) when a sudden voltage drop is observed, but there is minimal difference in the thermal domain (less than 1K). This emphasis the need for a multi-domain model

that can be used in case studies like load shifting and ancillary services (e.g., frequency regulation, ramp capacity)

VIII. CONCLUSION

In conclusion, this work presents the successful development and validation of a novel Computationally Efficient and Accurate Induction Machine (CEAIM) model, which offers superior accuracy and computational efficiency compared to existing models. By coupling the CEAIM model with HVAC equipment, such as pumps, heat pumps, and chillers, the proposed framework effectively captures the dynamic interactions between induction machines and thermo-fluid systems. The integration of electrical, thermal, and mechanical dynamics enables a comprehensive analysis of real-world scenarios, including grid interactions, which is critical for advancing energy-efficient and reliable HVAC systems. The case study demonstrated the potential of the proposed model to provide valuable insights into system performance under varying electrical conditions. These results highlight the utility of the developed framework for grid-interactive applications and pave the way for future research and optimization of coupled electrical and thermal systems in energy-critical domains. This work will be made open-source and released in the Modelica Buildings Library, providing a valuable tool for researchers and engineers studying advanced load shifting and ancillary services (e.g., frequency regulation, ramp capacity). The model also scales to support large-scale systems—such as district cooling/heating and data centers—in coordinating energy supply and demand.

ACKNOWLEDGMENT

All opinions expressed in this article are the author's and do not necessarily reflect the policies and views of DOE. The views expressed in the article do not necessarily represent the views of DOE and U.S. Government. The U.S. Government retains and the publisher, by accepting the article for publication, acknowledges that U.S. Government retains a nonexclusive, paid-up, irrevocable, worldwide license to publish or reproduce the published form of this work, or allow others to do so, for U.S. Government purposes. They acknowledge the use of OpenAI's ChatGPT for assistance in editing and refining the manuscript. The AI system was used for grammar enhancement and improving the clarity of certain sections. No technical content, equations, and original research findings were generated by AI.

DATA AVAILABILITY

Derived data supporting the findings of this study are available from the corresponding author on request.

REFERENCES

- [1] J. Martinez-Roman, R. Puche-Panadero, A. Sapena-Bano, C. Terron-Santiago, J. Burriel-Valencia, and M. Pineda-Sanchez, "Analytical model of induction machines with multiple cage faults using the winding tensor approach," *Sensors*, vol. 21, no. 15, p. 5076, Jul. 2021.
- [2] R. Parekh, *Ac Induction Motor Fundamentals*, document DS00887A, Microchip Technol., 2003.
- [3] V. Aviña-Corral, J. Rangel-Magdaleno, C. Morales-Perez, and J. Hernandez, "Bearing fault detection in adjustable speed drive-powered induction machine by using motor current signature analysis and goodness-of-fit tests," *IEEE Trans. Ind. Informat.*, vol. 17, no. 12, pp. 8265–8274, Dec. 2021.
- [4] D. Konovalov, I. Tolstorebrov, T. M. Eikevik, H. Kobalava, M. Radchenko, A. Hafner, and A. Radchenko, "Recent developments in cooling systems and cooling management for electric motors," *Energies*, vol. 16, no. 19, p. 7006, Oct. 2023.
- [5] A. Hmidet and O. Boubaker, "Real-time low-cost speed monitoring and control of three-phase induction motor via a voltage/frequency control approach," *Math. Problems Eng.*, vol. 2020, pp. 1–14, Apr. 2020.
- [6] M. Ali, A. Iqbal, M. R. Khan, and M. Khalid, "Ac–Ac converters," in *Power Electronics Handbook*. Amsterdam, The Netherlands: Elsevier, 2024, pp. 437–480.
- [7] C. Sheng, Q. Wang, T. Su, and H. Wang, "Induction motor torque closed-loop vector control system based on flux observation and harmonic current suppression," *Control Eng. Pract.*, vol. 142, Jan. 2024, Art. no. 105755.
- [8] M. Comanescu and L. Xu, "An improved flux observer based on PLL frequency estimator for sensorless vector control of induction motors," *IEEE Trans. Ind. Electron.*, vol. 53, no. 1, pp. 50–56, Feb. 2006.
- [9] Y. Tatte, "Torque ripple reduction with modified torque comparator in direct torque-controlled induction motor," *Electr. Eng.*, vol. 106, no. 4, pp. 4045–4058, Aug. 2024.
- [10] Y. SarcheshmehPour, T. Ryyppo, V. Mukherjee, and A. Jung, "Design of induction machines using reinforcement learning," 2023, *arXiv:2306.17626*.
- [11] Z. Danin, A. Sharma, M. Averbukh, and A. Meher, "Improved moth flame optimization approach for parameter estimation of induction motor," *Energies*, vol. 15, no. 23, p. 8834, Nov. 2022.
- [12] M. Magdy, S. Abu-Zaid, and M. A. Elwany, "Artificial intelligent techniques based on direct torque control of induction machines," *Int. J. Power Electron. Drive Syst. (IJPEDS)*, vol. 12, no. 4, p. 2070, Dec. 2021.
- [13] A. Marfoli, L. Papini, P. Bolognesi, and C. Gerada, "An analytical-numerical approach to model and analyse squirrel cage induction motors," *IEEE Trans. Energy Convers.*, vol. 36, no. 1, pp. 421–430, Mar. 2021.
- [14] E. Roshandel, A. Mahmoudi, S. Kahourzade, and W. Soong, "Analytical model and performance prediction of induction motors using subdomain technique," in *Proc. IEEE Energy Convers. Congr. Exposit. (ECCE)*, Oct. 2020, pp. 3815–3822.
- [15] M. Benninger, M. Liebschner, and C. Kreischer, "Comparison of population-based algorithms for parameter identification for induction machine modeling," *COMPEL-Int. J. Comput. Math. Electr. Electron. Eng.*, vol. 42, no. 4, pp. 878–892, Jun. 2023.
- [16] Y. Ma, L. Sun, Y. Xiao, J. Wang, J. Liu, and L. Zhou, "Analytical model of doubly-fed induction generator-motors for full-region operation analysis," in *Proc. 26th Int. Conf. Electr. Mach. Syst. (ICEMS)*, Nov. 2023, pp. 4472–4476.
- [17] I. Knežević, M. Čalasan, and T. Dlačić, "Novel analytical approaches for induction machine direct start-up speed-time curve modeling under fan load," *Electr. Eng.*, vol. 106, no. 2, pp. 1925–1938, Oct. 2023.
- [18] A. Bashir, M. A. Mohsin, M. Jazib, and H. Iqbal, "MINDTwin AI: Multiphysics informed digital-twin for fault localization in induction motor using AI," in *Proc. Int. Conf. Big Data, Knowl. Control Syst. Eng. (BdKCSE)*, Nov. 2023, pp. 1–8.
- [19] G. Istenes and K. Horváth, "Control algorithm development of electrical drives by using finite element model in connected MATLAB/simulink and JMAG framework," in *Proc. 18th Conf. Electr. Mach., Drives Power Syst. (ELMA)*, Jun. 2023, pp. 1–4.
- [20] S. M. A. Hajzber, A. J. Ali, A. H. Al-Rifaie, and A. K. Shanshal, "A comparative study for the performance operation of electric machine based on conventional and D-Q theories," *Int. J. Power Electron. Drive Syst.*, vol. 12, no. 3, p. 1304, Sep. 2021.
- [21] S. Khalghani, L. Aarniovuori, and J. Pyrhönen, "Evaluation of 5 kW converter-fed induction motor losses by analytical calculation," in *Proc. 29th Int. Workshop Electr. Drives, Adv. Power Electron. Electr. Drives (IWED)*, Jan. 2022, pp. 1–6.
- [22] T. Sapmaz, H. Eteci, I. Senol, and Y. Oner, "Optimization of three phase squirrel cage induction motor," in *Proc. Global Energy Conf. (GEC)*, Oct. 2022, pp. 148–153.
- [23] R. R. Singh, G. Bhatti, D. Kalel, I. Vairavasundaram, and F. Alsaif, "Building a digital twin powered intelligent predictive maintenance system for industrial AC machines," *Machines*, vol. 11, no. 8, p. 796, Aug. 2023.

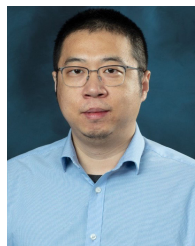
- [24] Q. Shen, Y. Zhou, and P. Zhang, "Physics-informed induction machine modelling," 2023, *arXiv:2309.16943*.
- [25] P. Tian, Q. Qu, Y. Cai, Y. Cheng, Y. Xu, S. Yao, and Y. Wang, "Modeling and simulation of induction motor based on time scale frame transformation," *J. Physics, Conf. Ser.*, vol. 1550, no. 4, May 2020, Art. no. 042013.
- [26] Z. Zhao, F. Fan, Q. Sun, H. Jie, Z. Shu, W. Wang, and K. Y. See, "Physics informed neural network-based high-frequency modeling of induction motors," *Chin. J. Electr. Eng.*, vol. 8, no. 4, pp. 30–38, Dec. 2022.
- [27] H. Husson, R. Thomas, and L. Garbuio, "2D finite element model of the audi e-Tron induction motor," in *Proc. IEEE Vehicle Power Propuls. Conf. (VPPC)*, Oct. 2021, pp. 1–6.
- [28] A. Zhao, H. Chen, C. Boßer, and M. Leksell, "Fem and cfd thermal modeling of an axial-flux induction machine with experimental validation," *Case Stud. Thermal Eng.*, vol. 53, Jan. 2023, Art. no. 103879.
- [29] M. Carbonieri, N. Bianchi, and L. Alberti, "Induction motor analysis using magnetostatic finite element simulations considering skewing," in *Proc. IEEE Int. Electric Mach. Drives Conf. (IEMDC)*, May 2019, pp. 147–153.
- [30] M. Kalla and B. Ponick, "Validation of a transient model for induction machines considering saturation and current displacement using transient FEM," in *Proc. 25th Int. Conf. Electr. Mach. Syst. (ICEMS)*, Nov. 2022, pp. 1–6.
- [31] F. Rezaee-Alam, A. Nazari Marashi, and S. Roozbehani, "Modified magnetic equivalent circuit model for magnetic field analysis of one cage-rotor induction motor used in electric submersible pumps," *IET Electric Power Appl.*, vol. 17, no. 6, pp. 802–812, Jun. 2023.
- [32] T. D. Lopes, A. Raizer, and W. V. Júnior, "Assessment of induction motor with rotor fault using a FEM-3D model," in *Proc. IEEE Power Energy Conf. Illinois (PECI)*, Mar. 2022, pp. 1–5.
- [33] J. Mei, Y. Zuo, C. H. T. Lee, and J. L. Kirtley, "Modeling and optimizing method for axial flux induction motor of electric vehicles," *IEEE Trans. Veh. Technol.*, vol. 69, no. 11, pp. 12822–12831, Nov. 2020.
- [34] A. Keyhani, W. Lu, and B. Proca, "Modeling and parameter identification of electric machines," in *Handbook of Automotive Power Electronics and Motor Drives*. Boca Raton, FL, USA: CRC Press, 2017, pp. 449–514.
- [35] P. C. Krause, O. Wasynczuk, S. D. Sudhoff, and S. Pekarek, *Analysis of Electric Machinery and Drive Systems*, vol. 2. Hoboken, NJ, USA: Wiley, 2002.
- [36] D. Lindenmeyer, H. W. Dommel, A. Moshref, and P. Kundur, "An induction motor parameter estimation method," *Int. J. Electr. Power Energy Syst.*, vol. 23, no. 4, pp. 251–262, May 2001.
- [37] J. M. Gutierrez-Villalobos, J. Rodriguez-Resendiz, E. A. Rivas-Araiza, and V. H. Mucino, "A review of parameter estimators and controllers for induction motors based on artificial neural networks," *Neurocomputing*, vol. 118, pp. 87–100, Oct. 2013.
- [38] M. Raina and H. A. Toliyat, "Parameter estimation of induction motors—A review and status report," in *Proc. IECON01. 27th Annu. Conf. IEEE Ind. Electron. Soc.*, vol. 2, Jul. 2001, pp. 1327–1332.
- [39] J. Montano, O. D. Garzón, D. A. Herrera-Jaramillo, O. D. Montoya, F. Andrade, and A. Tobon, "Estimating the parameters of a three-phase induction motor using the vortex search algorithm," *Iranian J. Sci. Technol., Trans. Electr. Eng.*, vol. 48, no. 1, pp. 337–347, Mar. 2024.
- [40] W.-M. Lin, T.-J. Su, and R.-C. Wu, "Parameter identification of induction machine with a starting no-load low-voltage test," *IEEE Trans. Ind. Electron.*, vol. 59, no. 1, pp. 352–360, Jan. 2012.
- [41] L. Peretti and M. Zigliotto, "Automatic procedure for induction motor parameter estimation at standstill," *IET Electric Power Appl.*, vol. 6, no. 4, pp. 214–224, Apr. 2012.
- [42] D. Klimenta, A. Hannukainen, and A. Arkkio, "Estimating the parameters of induction motors in different operating regimes from a set of data containing the rotor cage temperature," *Electr. Eng.*, vol. 100, no. 1, pp. 139–150, Mar. 2018.
- [43] H. R. Mohammadi and A. Akhavan, "Parameter estimation of three-phase induction motor using hybrid of genetic algorithm and particle swarm optimization," *J. Eng.*, vol. 2014, pp. 1–6, Jun. 2014.
- [44] U. Sengamalai, G. Anbazhagan, T. M. T. Thentral, P. Vishnuram, T. Khurshaid, and S. Kamel, "Three phase induction motor drive: A systematic review on dynamic modeling, parameter estimation, and control schemes," *Energies*, vol. 15, no. 21, p. 8260, Nov. 2022.
- [45] A. Véliz-Tejo, J. C. Travieso-Torres, A. A. Peters, A. Mora, and F. Leiva-Silva, "Normalized-model reference system for parameter estimation of induction motors," *Energies*, vol. 15, no. 13, p. 4542, Jun. 2022.
- [46] Y. Koubaa, "Application of least-squares techniques for induction motor parameters estimation," *Math. Comput. Model. Dyn. Syst.*, vol. 12, no. 4, pp. 363–375, Aug. 2006.
- [47] P. Kundur, "Power system stability," *Power Syst. Stability Control*, vol. 10, pp. 1–7, Aug. 2007.
- [48] P. M. Anderson and A. A. Fouad, *Power System Control and Stability*. Hoboken, NJ, USA: Wiley, 2008.
- [49] J. F. Kreider, P. S. Curtiss, and A. Rabl, *Heating and Cooling of Buildings: Design for Efficiency*. Boca Raton, FL, USA: CRC Press, 2009.
- [50] S. Sinha and S. S. Chandel, "Review of software tools for hybrid renewable energy systems," *Renew. Sustain. Energy Rev.*, vol. 32, pp. 192–205, Apr. 2014.
- [51] C. Marnay and G. Venkataramanan, "Microgrids in the evolving electricity generation and delivery infrastructure," in *Proc. IEEE Power Eng. Soc. Gen. Meeting*, May 2006, p. 5.
- [52] K. Nyström, P. Aronsson, and P. Fritzon, "Gridmodelica—A modeling and simulation framework for the grid," in *Proc. 45th Conf. Simul. Model. (SIMS)*, Apr. 2004, pp. 1–7.
- [53] M. Wetter and C. Haugstetter, "Modelica versus trnsys—A comparison between an equation-based and a procedural modeling language for building energy simulation," *Proc. SimBuild*, vol. 2, no. 1, 2006, pp. 1–8.
- [54] O. Gol, "Dynamic modelling of induction machines," Ph.D. dissertation, Dept. Elect. Electron. Eng., Univ. Adelaide, 1993.
- [55] (2025). *Modelica Buildings Library*. [Online]. Available: https://github.com/lbl-srg/modelica-buildings/tree/issue2948_MotorDriver_update
- [56] P. Fritzon, *Introduction to Modeling and Simulation of Technical and Physical Systems With Modelica*. Hoboken, NJ, USA: Wiley, 2011.
- [57] M. Wetter, M. Bonvini, T. S. Noudui, W. Zuo, and W. Tian, "Modelica buildings library 2.0," in *Proc. Building Simul. Conf.*, Hyderabad, India, Dec. 2015, pp. 387–394.
- [58] S. Huang, W. Zuo, and M. D. Sohn, "Amelioration of the cooling load based chiller sequencing control," *Appl. Energy*, vol. 168, pp. 204–215, Apr. 2016.
- [59] S. Huang, W. Zuo, and M. D. Sohn, "Improved cooling tower control of legacy chiller plants by optimizing the condenser water set point," *Building Environ.*, vol. 111, pp. 33–46, Jan. 2017.
- [60] *Dymola*. Accessed: Jun. 20, 2025. [Online]. Available: <https://www.3ds.com/products/catia/dymola>
- [61] M. Wetter, W. Zuo, T. S. Noudui, and X. Pang, "Modelica buildings library," *J. Building Perform. Simul.*, vol. 7, no. 4, pp. 253–270, 2014.
- [62] *Low Voltage General Purpose Motors*, ABB, Sweden, 2004.
- [63] *WEG*. Accessed: May 2, 2025. [Online]. Available: <https://www.weg.net/catalog/weg>
- [64] R. Le Fosse, "Dynamic modeling of induction motors in developing tool for automotive applications," Ph.D. dissertation, Dept. Control Comput. Eng., Politecnico di Torino, Turin, Italy, 2021.
- [65] A. Abbou, T. Nasser, H. Mahmoudi, M. Akherraz, and A. Essadki, "Induction motor controls and implementation using dsp," *WSEAS Trans. Syst. Control*, vol. 7, no. 1, pp. 26–35, 2012.



VISWANATHAN GANESH received the B.Tech. degree in electrical and electronics engineering from the SRM Institute of Technology, India, and the M.Sc. degree in sustainable electric power systems and electromobility from the Chalmers University of Technology, Sweden. He is currently pursuing the Ph.D. degree with the Department of Architectural Engineering, The Pennsylvania State University, University Park, PA, USA. His research interests include energy-efficient building systems, data center optimization, and intelligent control strategies for sustainable technologies.



ZHANWEI HE received the B.E. degree in architectural environment and equipment engineering from Xihua University, in 2015, and the M.S. and Ph.D. degrees in architectural engineering from The Pennsylvania State University, in 2018 and 2023, respectively. He is currently a Postdoctoral Scholar with the Sustainable Buildings and Societies Laboratory, The Pennsylvania State University. His research interests include resilient energy systems, cyber-physical power systems, district energy system modeling, HVAC systems, and the design and operation of microgrids and grid-interactive buildings.



SEN HUANG received the B.S. degree in architectural engineering from Donghua University, in 2008, the M.S. degree in architectural engineering from Tongji University, in 2011, and the Ph.D. degree in civil engineering from the University of Miami, in 2016. He is currently a Senior Research and Development Staff Member with Oak Ridge National Laboratory. He has worked intensively on control, optimization, and system modeling technologies with applications to the power grid, building systems, and building-to-grid integration. He received the 2022 International Building Performance Simulation Association-USA Regional Affiliate Emerging Contributor Award and the Best Paper Award from *Journal of Building Performance Simulation*.



JIANJUN HU received the B.S. and M.S. degrees in civil engineering from the University of South China, in 2003 and 2006, respectively, and the Ph.D. degree in Civil Engineering from Purdue University, West Lafayette, IN, USA, in 2014. He was a Visiting Researcher with the School of Mechanical Engineering, Purdue University, where he investigated algorithms for fast fluid dynamic simulation in buildings. Before joining the Lawrence Berkeley National Laboratory (LBNL), in February 2017, he was a Senior Research Engineer with the United Technologies Research Center, China, where he was the Principal Investigator for projects related to airflow management in supertall buildings, including stack effect mitigation, smoke control, and wind effects on HVAC systems. He also contributed to the development of virtual building testbeds using Modelica. He is currently an Engineering/Environmental Technology Researcher III with the Simulation Research Group of the Building Technology and Urban Systems Division, LBNL. His research focuses on the development of open-platform tools for building control system design and commissioning, and next-generation building energy and control simulation tools. His research interests include model predictive control, mixed-mode cooling strategies, dynamic modeling, and intelligent control solutions for optimizing building energy performance.



WANGDA ZUO received the B.S. and M.Eng. degrees in automation from Chongqing University, Chongqing, China, in 2000 and 2003, respectively, the M.Sc. degree in computational engineering from Friedrich-Alexander-University Erlangen-Nuremberg, Erlangen, Germany, in 2005, and the Ph.D. degree in mechanical engineering from Purdue University, West Lafayette, IN, USA, in 2010. He was an Assistant Professor with the University of Miami and a Computational Research Scientist with the Lawrence Berkeley National Laboratory. He is currently a Professor with the Department of Architectural Engineering, The Pennsylvania State University, University Park, PA, USA. He also has a joint appointment with the National Renewable Energy Laboratory, Commercial Buildings Group, Golden, CO, USA. He was a recipient of the ASCE ExCEED Fellowship, the IBPSA-USA Emerging Professional Award, the Eliahu I. Jury Early Career Research Award, the ASHRAE Distinguished Service Award, the Provost Research Award, and the SEEDS Leadership Award. He also served as the Founding Chair of the IBPSA-USA Research Committee and a Voting Member of the ASHRAE TC 4.7 Energy Calculations. He serves as a Treasurer and the Affiliate Director (representing USA) for the International Building Performance Simulation Association (IBPSA), the Chair and a Voting Member of the ASHRAE Technical Committee (TC) 7.4 Exergy Analysis for Sustainable Buildings, and the Vice Chair of ASHRAE (TC) 4.10 Indoor Environment Modeling.

• • •